Super-Resolution Imaging Reveals a Difference between SERS and Luminescence Centroids

Maggie L. Weber,[‡] Jonathan P. Litz,[†] David J. Masiello,[†,*] and Katherine A. Willets[‡,*]

[†]Department of Chemistry, University of Washington, Box 351700, Seattle, Washington 98195-1700, United States, and [‡]Department of Chemistry and Biochemistry, The University of Texas at Austin, 1 University Station A5300, Austin, Texas 78712, United States

ABSTRACT Super-resolution optical imaging of Rhodamine 6G surface-enhanced Raman scattering (SERS) and silver luminescence from colloidal silver aggregates are measured with sub-5 nm resolution and found to originate from distinct spatial locations on the nanoparticle surface. Using correlated scanning electron microscopy, the spatial origins of the two signals are mapped onto the nanoparticle structure, revealing that, while both types of emission are plasmon-mediated, SERS is a highly local effect, probing only a single junction in a nanoparticle aggregate, whereas luminescence probes all collective plasmon modes within the nanostructure. Calculations using the discrete-dipole approximation to calculate the weighted centroid position of both the $|E|^2/|E_{inc}|^2$ and $|E|^4/|E_{inc}|^4$ electromagnetic fields were compared to the super-resolution centroid positions of the SERS and luminescence data and found to agree with the proposed plasmon dependence of the two emission signals. These results are significant to the field of SERS because they allow us to assign the exact nanoparticle junction responsible for single-molecule SERS emission in higher order aggregates and also provide insight into how SERS is coupled into the plasmon modes of the underlying nanostructure, which is important for developing new theoretical models to describe SERS emission.

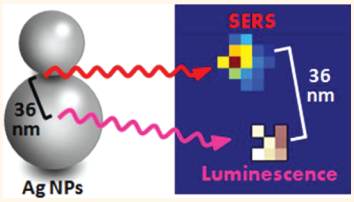

KEYWORDS: silver luminescence · surface-enhanced Raman scattering · hot spots · discrete-dipole approximation · plasmon

Many theoretical and experimental studies of metallic nanostructures have illustrated the importance of nanoparticle shape, size, and degree of aggregation upon the surface-enhanced Raman scattering (SERS) phenomenon, particularly the electromagnetic field enhancement in nanoparticle junctions.[1−6] Fully understanding how these variables, along with excitation wavelength and polarization, affect optical response will allow us to design reliable, robust SERS substrates. The challenge with characterizing SERS substrates is that the bulk of the enhancement occurs in "hot spots" located in the junctions between adjacent nanoparticles.[5,7] The small size of these hot spots in comparison to the diffraction limit of light, which restricts optical imaging resolution to roughly half the wavelength of the probing light, prevents optical imaging of hot spot size and geometry. Recently, super-resolution imaging was applied to the SERS problem in order to defeat the diffraction limit of light and probe the local behavior of molecules adsorbed to nanoparticle surfaces.[8−10] Our group and others have shown that a correlation exists between the super-resolution determined spatial origin of the SERS signal and the intensity of the measured SERS. This demonstrates the power of super-resolution imaging for understanding these complex nanoscale systems.[8−10]

In our previous work, we used super-resolution optical imaging to locate and track the spatial origin of the SERS signal from Rhodamine 6G (R6G) molecules on sodium-chloride-aggregated silver nanoparticle aggregates, taking advantage of the strong on/off signal fluctuations inherent to single- or few-molecule SERS.[8] During the periods when no SERS was observed, we found a weak silver photoluminescence background signal.[8] Using super-resolution imaging, we fit the spatial origin of both the SERS and luminescence signals and found that in some cases the strongest SERS emission was colocalized with the luminescence (within 5−10 nm), while in other cases, the position of the two signals was spaced by more than 50 nm. We speculated that the offset between the two signals was related to the structure of the nanoparticle aggregates, which are known to be diverse in these randomly assembled silver colloids.

To investigate the role of nanoparticle structure, we repeated this initial study using indium tin oxide (ITO)-coated glass coverslips as the substrate to enable correlated structural analysis with a scanning electron microscope (SEM).[9] However, the change in substrate and dielectric environment

* Address correspondence to masiello@chem.washington.edu, kwillets@mail.utexas.edu.

Received for review December 26, 2011 and accepted January 16, 2012.

Published online January 16, 2012
10.1021/nn205080q

© 2012 American Chemical Society

modified the chemical dynamics of the system: where the on/off behavior of R6G SERS in the single-molecule concentration regime was exploited in previous studies, the comparative experiments on ITO glass showed fluctuating spectral features of R6G on top of an unstable background spectrum from sodium citrate, the reducing agent which caps the silver colloids during synthesis.[11−13] Figure 1A illustrates the type of R6G SERS spectra observed on ITO using NaCl-aggregated silver colloids. While the intensity time trace (Figure 1A, bottom) shows on/off signal behavior, there are peaks evident in the SERS spectra even when the signal intensity is low (Figure 1A, top). Moreover, the spectra corresponding to times when the SERS signal is "on" in the time trace (*e.g.*, 74 s) cannot be clearly identified as R6G. Thus, our reported SERS centroids are biased by a contribution from this unstable citrate background, and we are unable to assign the spatial origin of the silver luminescent background. This prevents us from explaining why the two signals are colocalized in some cases and offset in others.

In the present study, we address this problem by modifying the colloid aggregation chemical from sodium chloride to sodium bromide in order to improve citrate displacement, thereby eliminating any spectral signatures of citrate.[8,14,15] Figure 1B shows data collected from an R6G-labeled silver colloid sample aggregated with NaBr. The intensity time trace shows the same on/off behavior as in Figure 1A, but the associated spectra show characteristic R6G peaks only during the "on" times and a clean flat background during the "off" times (Figure 1B, bottom). Even though the spectra are featureless during the "off" times, we note that the intensity of the time trace never goes down to zero background, which indicates that silver photoluminescence is still present in the sample.[8] Thus, using this new nanoparticle aggregation strategy, we are able to relate the spatial origin of the observed luminescence to both the measured SERS signal from an adsorbed dye (as determined by super-resolution imaging) and the structure of the overall nanoparticle aggregate (as determined by electron microscopy). Computationally, Maxwell's equations are solved *via* the discrete-dipole approximation (DDA) to determine the continuum electromagnetic scattering properties of the metal nanoparticle aggregates.[16] From these calculations, the expected site of emission for plasmon-mediated processes following either $|\mathbf{E}|^2$ or $|\mathbf{E}|^4$ enhancement mechanisms is compared to the experimentally measured SERS and luminescence signals.

SERS super-resolution imaging is performed using wide-field epi-illumination with 532 nm excitation as described below. For each SERS-active aggregate of interest, we simultaneously collect a series of CCD images (1000 total at 0.1 s integration) and spectra (100 total at 1 s integration). The diffraction-limited

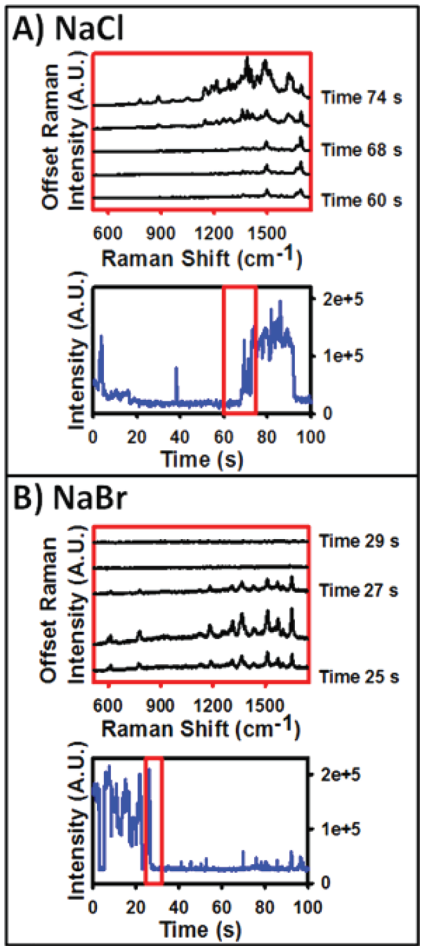

Figure 1. (A) Time trace of R6G SERS from a NaCl-aggregated silver colloid (bottom) and the associated SERS spectra for the red boxed region in the time trace (top). (B) Same as in (A) but for R6G SERS from a NaBr-aggregated silver colloid.

spot in each optical image, corresponding to a single SERS-active aggregate of interest, is fit to a two-dimensional Gaussian and its centroid determined so we can monitor the position of the SERS signal and the luminescence as a function of time.[8,9] This method, known as point spread function (PSF) fitting, was determined to be the most robust in low signal-to-noise situations such as single-molecule studies by Cheezum *et al.*,[17] and recently, Selvin *et al.* have reported PSF fitting with ~1 nm resolution providing a significant advantage over the diffraction limit.[18,19] The PSF fit equations and method used in this article have been explicitly outlined in previous works.[8,9] Briefly, the Gaussian equation used to model the shape and intensity of a diffraction-limited spot is

$$I(x,y) = z_0 + I_0 e^{\left[-\frac{1}{2}\left[\left(\frac{x-x_0}{s_x}\right)^2 + \left(\frac{y-y_0}{s_y}\right)^2\right]\right]} \quad (1)$$

where I is the intensity for a given position (x,y) in space, z_0 is the background intensity, I_0 is the intensity at the center of the Gaussian fit, $s_{x,y}$ are the standard

deviation in x and y, respectively, and x_0 and y_0 are the centroid of the fit (see Supporting Information for more details). Individual frames in the image stack are assigned as originating from either nanoparticle luminescence or a combination of luminescence and SERS using the corresponding spectral data. A threshold is drawn in the intensity time trace such that all intensity events above the threshold have correlated Raman spectra exhibiting characteristic R6G peaks and all events below the threshold correspond to luminescence emission only (see Figure S-1 in Supporting Information for all time traces with thresholds and associated spectra for data described below). For all frames designated as luminescence emission only (*i.e.*, below the intensity threshold), a Gaussian function is fit to each emission pattern in order to determine its centroid position (*i.e.*, x_0 and y_0). The average position of the luminescence centroid is calculated over all frames and checked for positional stability by calculating the standard deviation in the centroid position. For all aggregates discussed in this article, the standard deviations of the fit of the luminescence centroids ranged from 1 to 6 nm (Figures S-3 and S-5). The theoretical accuracy of the luminescence centroid is 0.9 nm based on our pixel size, standard deviation of the fitted Gaussian, and signal-to-noise (Table S-1).[19] Once we establish that the luminescence originates from a single, stable location for a given SERS-active colloidal aggregate, we arbitrarily set the average position of the luminescence centroid to (0,0).

Next, all frames with intensities above the threshold are processed to exclude the contribution from the luminescence and then fit as a single 2-D Gaussian to extract the SERS centroid.[8] Although this analysis assumes that only a single R6G is contributing to the signal at a given time, we cannot exclude the possibility of multiple emitters contributing simultaneously to a single image. In this case, the emission centroid would be the superposition of the location of the different emitting species. We have chosen our dye concentration to be in a similar range to those used in single-molecule SERS proof-of-concept studies with identical colloid synthesis (Lee and Meisel method) in order to favor the likelihood that only a single molecule is present on the nanoparticle surface.[20−22] Moreover, in the case of two emitters present on the surface, we note that the fluctuating nature of the SERS signal would lead to times at which both molecules are emitting, times at which one or the other is emitting, and times when neither is emitting. Using a bianalyte technique, Van Duyne and co-workers have shown that even at high dye concentrations (~100 molecules per nanoparticle) signal is only observed from one molecular species at a time, suggesting that a single hot spot can only be occupied by one molecule at a time.[23] Thus, for events corresponding to two molecules emitting at the same time, the two molecules would have to occupy spatially distinct hot spots. We expect this to produce three distinct centroids, two of which correspond to the location of each unique hot spot determined when only a single molecule is emitting, as well as the superposition of the two centroids determined during times at which both are emitting simultaneously. In the data presented here, we do not observe multiple distinct SERS centroids, although we have previously reported this phenomenon in another system.[9] Thus, our data support that the SERS originates from a single emitter, although bianalyte studies are underway to rigorously verify this.

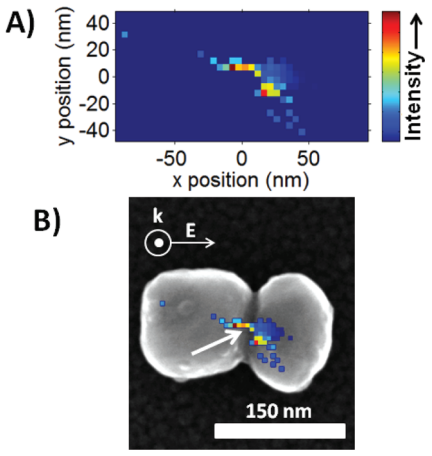

Figure 2. (A) SERS spatial intensity map, showing the relationship between the SERS intensity (color scale) and the spatial origin of the SERS signal with respect to the luminescence centroid at (0,0). (B) Overlay of the SERS spatial intensity map and luminescence centroid (tip of white arrow) with an SEM image of the SERS-active silver nanoparticle aggregate.

After we have determined the SERS centroid positions for all frames above the intensity threshold, the centroid data are binned to create a two-dimensional position histogram (0.1 pixel or 4.6 nm bin size). This bin size is chosen based on the theoretical resolution of ~5 nm for the weakest SERS signal (Table S-1). We then calculate the average SERS intensity for all points within a bin to create a SERS spatial intensity map, which illustrates where regions of most intense SERS scattering occur; an example is shown in Figure 2A (see Supporting Information for more details regarding fitting procedure and data processing).

RESULTS AND DISCUSSION

For the data shown in Figure 2A, there are two regions of "hot" SERS activity, located on either side of the luminescence centroid at (0,0). The corresponding SEM image, shown in Figure 2B, reveals that the SERS-active nanoparticle is a dimer, oriented parallel to the excitation polarization.

Theoretical calculations in the literature have long indicated that the most intense SERS is expected to originate from the junction between aggregated nanoparticles, especially for a dimer excited along its long

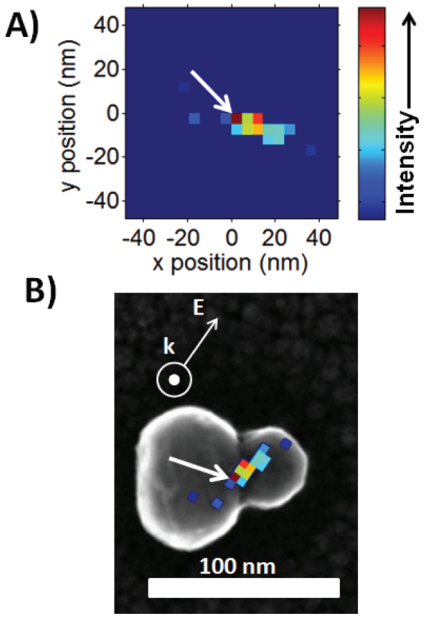

Figure 3. (A) R6G SERS spatial intensity map and associated luminescence centroid (arbitrarily set to (0,0) and indicated by a white arrow). (B) Overlay of luminescence centroid and spatial intensity map with correlated nanoparticle SEM image. Note that the spatial intensity map has been rotated to match the orientation of the SEM image.

axis.[4,6,24−26] In the case of dimers with small gaps between them, the highest electromagnetic field enhancements are calculated to fall on the edges of the two nanoparticles that face the junction, with a minimum in the gap itself.[27] We note that the spatial intensity map in Figure 2A has a spatial distribution of the SERS signal that is similar to the predicted electromagnetic field distribution for nontouching dimers. For this reason, we overlay the SERS spatial intensity data onto the SEM data in Figure 2B such that the two regions of strong SERS are located on either side of the junction, consistent with the expectations from theory. Although this overlay is not mathematically rigorous, it agrees with theoretical expectations and serves as a reasonable initial guess. Attempts to quantitatively assign the spatial origin of the SERS centroid *via* triangulation using alignment markers produces an accuracy of ~50 nm, which is insufficient for assigning the hot spot location. We observe some variation in the position of the SERS emission centroid, which we attribute to a mobile dipole on the nanoparticle surface as discussed in our previous work.[8] On the basis of our super-resolution fits, we see colocalization of the average position of the luminescence signal (tip of white arrow) with the strongest SERS, indicating that if our placement of the spatial intensity map is correct, then the luminescence signal is also associated with the junction between the two nanoparticles in this dimer.

Figure 3 presents the SERS spatial intensity map (Figure 3A) and associated structure (Figure 3B) of an asymmetric dimer with one particle significantly larger

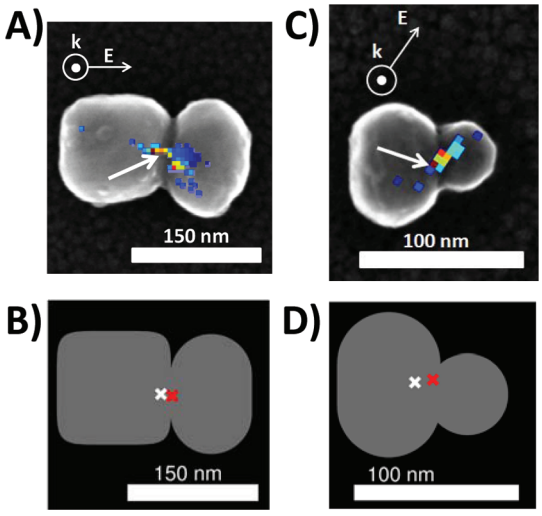

Figure 4. (B,D) DDA calculations for experimental nanoaggregates in Figures 2 and 3 (reproduced in A and C, respectively). The ε^2 centroids are identified by white Xs, and ε^4 centroids are identified by red Xs. The polarization angles for B and D match those of their corresponding experimental structures.

than the other and whose long axis is oriented roughly 45° from the laser polarization. As before, we place the regions of strongest SERS signal on either side of the junction, consistent with the presence of a small gap. In this case, we observe that placing the SERS centroid on the nanoparticle junction leads to a small (~10 nm) offset in the luminescence centroid away from the junction and toward the larger nanoparticle.

To quantitatively assign the position of the SERS centroid, we use our SEM images to construct a three-dimensional numerical representation of each nanoparticle aggregate in DDA. From the output of DDA, one may construct a near-field mapping of the electromagnetic field enhancement surrounding the nanostructure.[2−5,28,29] We calculated the ratio of the magnitude of the local electric field **E** to the magnitude of the incident electric field $\mathbf{E}_{inc}$, $\varepsilon = |\mathbf{E}|/|\mathbf{E}_{inc}|$, on a grid with 1 nm^3 resolution in the region that encapsulates the near-field behavior of **E** at an excitation wavelength of 532 nm. The near-field map of ε was translated into a far-field centroid position, $\langle \mathbf{X} \rangle$, by calculating the weighted average of the position in the enhanced electromagnetic field distribution. The weighting factor was ε^2 for luminescence and ε^4 for SERS:

$$\langle \mathbf{x} \rangle(\omega) = \frac{\sum_i \mathbf{x}_i f(\varepsilon(\mathbf{x}_i, \omega))}{\sum_i f(\varepsilon(\mathbf{x}_i, \omega))} \qquad (2)$$

$$f(\varepsilon) = \begin{cases} \varepsilon^2 \text{ for luminescence} \\ \varepsilon^4 \text{ for SERS} \end{cases}$$

We chose to model both the ε^2 and ε^4 centroid positions because the former is associated with surface-enhanced fluorescence, while the latter is associated with SERS.[4,30]

Figure 4A,B shows the experimental and theoretical results for the first dimer structure from Figure 2. In this case, both the calculated ε^2 and ε^4 centroids are localized near the junction of the dimer in the theoretical calculations (Figure 4B). SERS is expected to track with the ε^4 centroid, and we find excellent agreement between the location of the calculated ε^4 centroid and our placement of the SERS spatial intensity map in Figure 4A. We also note that the location of the luminescence agrees with the location of both the calculated ε^2 and ε^4 centroids. Figure 4C,D shows the results for the heterodimer structure from Figure 3. Again, the ε^4 centroid is located in the junction between the two nanoparticles and is consistent with our experimental SERS assignment. Interestingly, the calculated ε^2 centroid is shifted away from the junction and toward the larger nanoparticle, similar to the luminescence centroid in our experimental data.

In our previous work, we speculated that colocalized SERS and luminescent centroids were indicative of a single hot spot dominating both the SERS emission and the silver luminescence.[8] This hypothesis is substantiated by the DDA calculations presented in Figure 4, with one small caveat. In the case of SERS emission, the signal is strongly coupled into and emitted by the longitudinal plasmon mode, based on polarization measurements performed by our group and others.[31−33] In Figure 4A,B, the longitudinal plasmon mode is aligned with the excitation polarization, which leads to strong excitation of this mode and the calculated centroids appearing colocalized with the nanoparticle junction. This is consistent with the proposed model of a single hot spot (or plasmon mode) dominating the two measured centroids.

On the other hand, the nanoparticle shown in Figure 4C,D is excited by light polarized at 45° to the long axis of the dimer. This results in excitation of both longitudinal and transverse dipolar plasmon modes (in addition to higher order modes), which can both contribute to the calculated ε^2 and ε^4 centroids. In the case of the ε^4 centroid, the enhanced electromagnetic field of the longitudinal mode is sufficiently high that it dominates the centroid calculation when raised to the fourth power; however, in the ε^2 centroid calculation, the contribution from the transverse plasmon associated with the larger nanoparticle contributes appreciable enhancement to the calculated centroid, shifting it away from the junction. Experimentally, if the luminescence is coupled to multiple plasmon modes, then its centroid will be a weighted superposition of the different emission sites associated with these different modes, analogous to multiple molecules emitting in a single diffraction limited spot. For the data shown in Figure 4C,D, we propose that the luminescence is emitted *via* coupling to both the longitudinal and transverse plasmons in the dimer nanostructure, which shifts the measured luminescence centroid toward the leftmost nanoparticle, as observed experimentally.

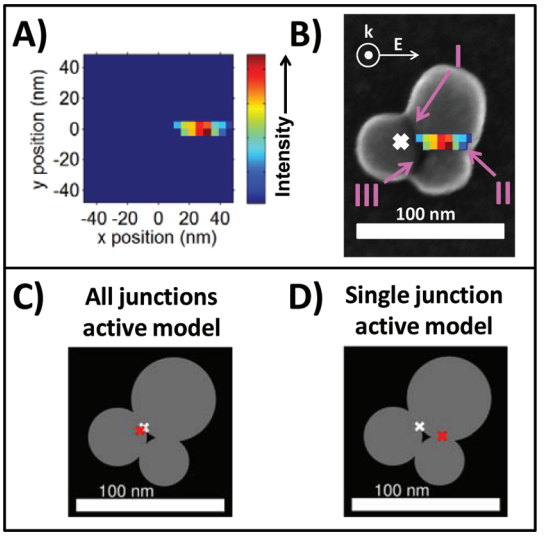

Figure 5. (A) SERS spatial intensity map with luminescence centroid arbitrarily set to (0,0). (B) Overlay of luminescence centroid (white x) and SERS spatial intensity map with SEM image of the nanoparticle structure. (C) DDA calculation of the ε^2 (white x) and ε^4 (red x) centroid positions for the modeled trimer, accounting for plasmonic enhancement over the entire structure. (D) DDA calculation of the ε^4 (red x) centroid position for the modeled trimer, accounting for plasmonic enhancement at the lower right junction only. The ε^2 (white x) centroid is the same as in (C).

Next, we present a nanoparticle trimer in Figure 5, in which the SERS and luminescent centroids are offset by more than 30 nm. Käll and co-workers have modeled a similar structure and found that all three junctions in a grouped trimer should experience enhanced electromagnetic fields capable of supporting SERS.[34] However, the spatial intensity map in Figure 5A shows only a single SERS hot spot, suggesting that only a single junction is SERS-active in the trimer. DDA calculations on this nanostructure show that the calculated ε^2 and ε^4 centroids are strongly colocalized and associated with the leftmost nanoparticle near the junction labeled I (Figure 5B,C). However, this calculation assumes that the emitter is sampling all plasmon modes across the nanoparticle trimer, and thus the centroid is a weighted superposition of these different emission sites. While we believe this to be the case for nanoparticle luminescence, SERS is expected to be a local effect in which the emission of the molecule is dominated by the hot spot in which it is located.[9,10,33,35] In this case, the geometries of junctions I and III are incongruous with the horizontal alignment of the SERS spatial intensity map, indicating that these junctions are not responsible for the measured SERS activity. Junction II not only has the proper horizontal alignment that matches with the line shape of the spatial intensity map but also results in the luminescence centroid positioned on the leftmost nanoparticle, as predicted by the DDA calculations. If we recalculate the

ε^4 centroid, assuming the molecule is only sampling the plasmon mode associated with junction II, we find excellent agreement between the spacing of the two centroids across the trimer surface (Figure 5D). These data show that SERS is emitted *via* coupling to a *local* plasmon mode, dictated by the position of the analyte molecule on the surface, while luminescence is best described by the *collective* plasmon enhancement, averaged over multiple plasmon emission sites over the entire nanoparticle structure. For this reason, it is possible for the SERS and luminescence centroids to be offset by many tens of nanometers, as we had previously speculated.[8]

To further support this idea, we present two additional examples in Figure 6, in which the SERS and luminescent centroids are offset from one another by tens of nanometers. For the trimer shown in Figure 6A, we again observe only a single SERS hot spot, despite the presence of two possible SERS-active junctions. As with the previous trimer example, we can use the luminescence centroid to assist us in assigning the SERS-active junction. Given our expectation that the luminescence centroid reports a superposition of all plasmon modes in the nanostructure, we expect the centroid position to be strongly influenced by both junctions in the trimer. In this case, junction I is "hotter" than junction II, given the polarization of the excitation light being aligned strongly with the long axis of this junction; thus, the luminescence centroid is expected to be weighted toward junction I. However, the presence of junction II will contribute some small, but significant, plasmon enhancement, biasing the luminescence centroid vertically upward. If we now look at the spatial intensity map in Figure 6A, we observe that the luminescence centroid is vertically displaced from the SERS hot spot. If we assign junction II as the SERS-active junction, the luminescence centroid would fall on the edge of the upper-most nanoparticle, which is inconsistent with plasmon-mediated emission. On the other hand, if junction I is occupied by the R6G, then the luminescence centroid falls on that same junction, just higher in the vertical direction, as expected. Thus, on the basis of our insight about the luminescence centroid, we assign junction I as the SERS-active junction in this example. Given the size and complexity of this nanostructure, it was too computationally demanding to calculate ε^2 and ε^4 centroids for a full-scale model of this aggregate. However, a rough theory calculation can be found in the Supporting Information and shows reasonable agreement with our assignment of junction I as the SERS-active junction. As with the dimer from Figure 3, the location of the luminescence centroid agrees better with the calculated ε^2 centroid.

As a final example, Figure 6B shows an asymmetric nanoparticle dimer, in which the SERS and luminescent centroids are displaced by nearly 50 nm. This example further strengthens our argument that the

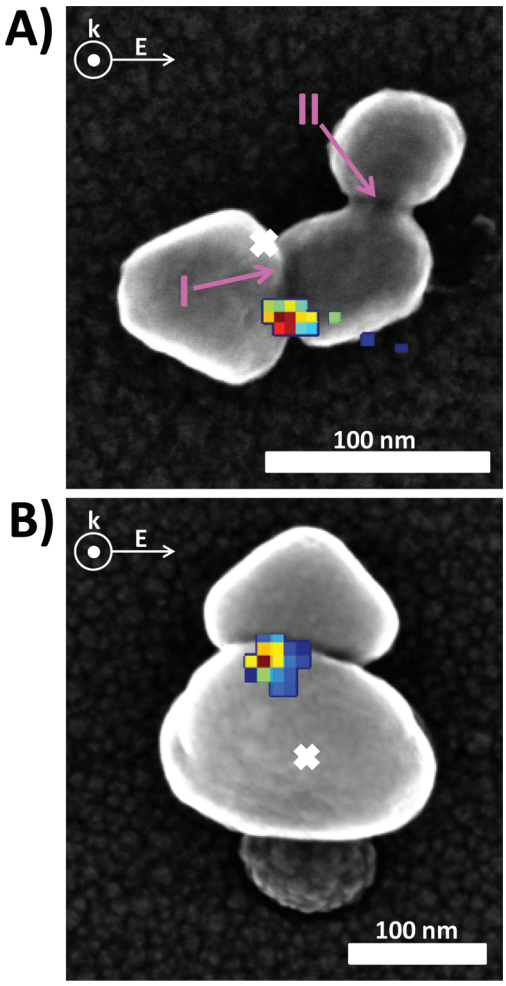

Figure 6. (A) Overlay of SERS spatial intensity map and luminescent centroid (white x) on the SEM structure of a trimer. (B) Overlay of SERS spatial intensity map and luminescent centroid (white x) on the SEM structure of a vertically oriented asymmetric dimer.

luminescence is not dominated by the "hot spot" in the nanostructure, but rather reports on a weighted superposition of all actively excited plasmon modes. If we position the SERS data such that it is near the junction between the two particles, the luminescence centroid clearly favors the much larger nanoparticle on the bottom (the lowest dark sphere is believed to be substrate material or some other nonplasmonic contaminant). For the SERS, the emission strongly couples to the junction-associated longitudinal plasmon mode, even though this mode is inefficiently excited by the horizontally polarized light.[33] On the other hand, the nanostructure is expected to support both longitudinal and transverse plasmon modes, both of which can couple to the luminescence. For a vertically oriented dimer excited with horizontally polarized light, little electromagnetic field enhancement would be expected in the junction.[2] Consequently, the transverse dipolar and multipolar plasmon modes will have a much stronger impact on the overall plasmonic enhancement of the nanoparticle.[2] In this case, we

predict that the transverse plasmon associated with the larger nanoparticle couples more strongly with the 532 nm excitation light, shifting the luminescence centroid toward the lower nanoparticle. The effect of the contaminant dielectric sphere in contact with the lower nanoparticle may also impact the plasmon modes of the aggregate, although this is more challenging to describe, given the uncertainty of its size and composition.

One challenge with SEM structural characterization is the loss of three-dimensional information about the exact geometry of the gap structure. In this case, the larger nanoparticle has curvature that extends over the lower edge of the triangular nanoparticle, obscuring the junction. This missing geometric information about the junction may help explain why strong SERS is observed from this nanostructure, even though the junction appears oriented parallel to the excitation light.

Notably, in several of our examples, the calculated ε^2 centroid agrees better than the ε^4 centroid with the experimentally determined luminescence centroid. One question that remains open is why nanoparticle luminescence would be an ε^2 process. Typical nanoparticle plasmon-mediated ε^2 processes include Rayleigh scattering and surface-enhanced fluorescence. In the case of the former, the scattering intensity depends on the polarizability of the nanostructure, which leads to the ε^2 dependence.[29,36] In the latter case, the intensity of the excitation field is enhanced (ε^2) but the emission is dominated by changes in the radiative rate due to the presence of the metal nanoparticle.[36−39] In the case of luminescence, we speculate that the excitation field is enhanced (ε^2), but that the emission does not experience a similar enhancement. As evidence that the excitation field is enhanced, we have observed that the intensity of the luminescence depends on the polarization of the excitation light, which is expected in the case of a plasmon-mediated excitation process.[26,40] On the other hand, we do not observe any overlap between the broad silver luminescence and the measured plasmon resonance spectra for the aggregates, indicating that the two processes are not intimately related; this is in stark contrast to gold luminescence, in which the emission spectrum mirrors the plasmon resonance spectrum in gold nanorod structures.[41]

To understand this in more detail, it is worth considering the possible origins of the luminescence signal in colloidal silver nanoparticles. Although the existence of the signal is widely accepted by researchers, the responsible mechanism remains a subject of debate.[42−46] Current hypotheses in the literature propose that luminescence is due to interband transitions, fluorescence of chemi- or physisorbed molecules on silver colloids, or small fluorescent clusters of silver atoms on the surface of larger colloids.[42,44−52] In addition to these mechanisms, we must also consider the possibility of electronic Raman scattering from "dirty" silver nanoparticles, as described by Brus and others.[53−55] We rule out the first two mechanisms as follows: first, the interband transition in silver is toward the ultraviolet and is not expected to be resonant with our 532 nm excitation light, suggesting that direct excitation of silver is not the responsible mechanism.[41,56] Second, fluorescence from adsorbed molecules is also unlikely, as we and others have observed luminescence in the absence of fluorescent dye molecules on the nanoparticles.[8,43] In the odd case of carbon contamination on the nanoparticle surface, we observe the appearance of sharp Raman bands rather than a broad, stable luminescence, suggesting that adsorbed molecules would produce strong SERS rather than luminescence if they were, in fact, resonant with our excitation light.[57]

The hypothesis that luminescence is caused by small clusters of silver atoms on the surface of the larger metal colloids remains a well-accepted mechanism to describe the photoluminescence background.[42,48,49] Recent reports in the literature have shown successful syntheses of isolated silver atom clusters (2−39 atoms) that are strongly photoluminescent, supporting the idea that small silver clusters on the nanoparticle surface could be responsible for the observed photoluminescence.[58−60] Work from Dickson and co-workers on Ag|Ag_2O films observed the formation of luminescent spots upon photoactivation,[50] while more recent work from Lupton and co-workers has shown similar behavior on the surface of silver island films;[49] in both cases, the luminescence was assigned to the formation of silver clusters on the film surface. A recent report from Wang and Palmer used aberration-corrected scanning transmission electron microscopy to show that so-called "magic number" gold nanoparticles are covered with single gold adatoms as well as gold adatom clusters, indicating that even in closed shell systems, the surface can be defected, rather than atomically smooth.[61] Although a similar study has not been done for silver nanoparticles, this study supports the idea that silver adatom clusters should be stable on the surface of larger nanoparticles. Here, we speculate that small, several-atom clusters could form spontaneously on the surface of the silver nanoparticles and produce the observed luminescence. Given that the nanoparticles are prepared in ambient air and not protected from oxygen, the photoreduction of surface silver oxides may play a role, as suggested by Dickson and co-workers.[50,51] Questions that remain are (1) why the luminescence emission from these clusters would not couple to the nanoparticle plasmons, leading to ε^4 enhancement, and (2) why the clusters would behave as entities independent from the "bulk" metal surface, to which they are in intimate contact.

The final mechanism involves electronic Raman excitation of silver, catalyzed by defect sites on the nanoparticle surface.[62] Brus *et al.* explained the presence of

the well-known continuum background that accompanies single-molecule SERS by characterizing the Raman analyte as a defect site that couples to the bulk silver and scatters with an ε^2 dependence, consistent with our data. In their work, they found that this continuum was only observed when the R6G molecule was present, acting as a defect site, due to the highly crystalline surfaces on their as-prepared nanoparticles. However, if our nanoparticles have surface defects, such as the clusters described above, we could expect these clusters to act as nucleation sites for electronic Raman scattering. This type of behavior was also reported for silver films and small silver clusters in the absence of adsorbed dyes.[62−64]

While we cannot rigorously prove the origin of the luminescence background in our samples, our results are consistent with the models of both luminescent clusters and surface defect-mediated electronic Raman excitation of the silver metal.[42,46,48,49] More investigation is needed to understand this phenomenon, but our results demonstrate that the luminescence is clearly linked to the collective excitation of plasmons within the silver nanoparticle aggregates, with the centroid reporting on a weighted superposition of different plasmon-mediated emission sites. Perhaps more important is the fact that the luminescence centroid location allows us to assign the SERS-active junction in the case of higher-order aggregates (*e.g.*, trimers, tetramers, *etc.*) by using theoretical calculations of plasmonic enhancement distributed over the entire nanoparticle structure (as in Figures 5 and 6). This is of critical importance as we continue to develop super-resolution imaging as a tool for studying SERS substrates, especially at the single- or few-molecule level.

CONCLUSIONS

In conclusion, we have shown that the offset between the luminescence and SERS centroids can be explained by different coupling mechanisms between each emission process and the plasmonic enhancement provided by the nanoparticle. In the case of SERS, the emission couples into a local plasmon mode, dictated by the position of the molecule on the nanoparticle surface, while the plasmon-mediated silver luminescence is coupled into all active plasmon modes in the nanoparticle structure. These different mechanisms lead to an offset between the SERS and luminescence centroids in our super-resolution imaging data when nanoparticles support more than one dominant plasmon mode. Our results also suggest that the luminescence is enhanced *via* an ε^2 mechanism, although further work is needed to rigorously prove this and explain the mechanism behind it.

METHODS

SERS samples are prepared using citrate-reduced silver colloids synthesized *via* the Lee and Meisel method.[20] A 2 mL aliquot of these as-prepared colloids is incubated with R6G dye (1 nM final concentration) and aqueous sodium bromide (9.52 mM final concentration) for 1 h. After incubation, 4 μL of this solution and a small amount of Spherotech Blue Sky fluorescent marker beads used for alignment purposes are drop-cast onto an ITO-coated glass coverslip that has been patterned with an aluminum alphanumeric grid, as described in previous work, to facilitate correlated studies.[9]

Samples are first analyzed optically using an inverted Olympus IX-71 microscope with linear-polarized 532 nm laser excitation in epi-illumination. After passing through a 550 nm longpass filter to block Rayleigh scattered laser light, the resulting emission is split with a 50/50 beamsplitter that sends half of the signal to a Princeton Instruments ProEM 512 electron-multiplying charge-coupled device (CCD) camera for SERS imaging, while the other half is dispersed by a PI ACTON SpectraPro 2500i spectrograph coupled to a Spec-10 camera for spectral acquisition. The SERS images consist of photons with wavelengths longer than 550 nm, allowing us to collect both luminescence and SERS signals with a single detector. The wavelength overlap between the two signals at 532 nm excitation precludes separation of the two signals into separate spectral domains. Each CCD pixel corresponds to 46 nm in the sample, calibrated using a USAF test target. Correlated structural data are collected using a high-resolution Hitachi S-5500 SEM (30 kV accelerating voltage). Complete sample preparation and experimental details are provided in the Supporting Information.

Acknowledgment. We thank Spherotech for the generous gift of fluorescent nanospheres used as alignment markers. We also thank the National Science Foundation (Grant No. 0821312) for funding the Hitachi S-5500 scanning electron microscope/scanning transmission electron microscope used in this work, and Texas Materials Institute for supporting this facility. This material is based on work supported by the Welch Foundation under Award No. F-1699 (K.A.W.), the Air Force Office of Scientific Research under AFOSR Award No. FA9550-09-0112 (K.A.W.), the National Science Foundation Graduate Research Fellowship under Grant No. DGE-0718124 (J.P.L.), and the University of Washington Royalty Research Fund (D.J.M.).

Supporting Information Available: Experimental details, SEM images of aggregates without overlays and their associated spectral and intensity timetrace data, super-resolution fitting technique details, scatter plots for luminescence centroid data, sample resolution calculation for Figure 2B luminescence and SERS data, and the DDA result for the aggregate in Figure 6A. This material is available free of charge *via* the Internet at http://pubs.acs.org.

Conflict of Interest: The authors declare no competing financial interest.

REFERENCES AND NOTES

1. Wustholz, K. L.; Henry, A.-I.; McMahon, J. M.; Freeman, R. G.; Valley, N.; Piotti, M. E.; Natan, M. J.; Schatz, G. C.; Van Duyne, R. P. Structure−Activity Relationships in Gold Nanoparticle Dimers and Trimers for Surface-Enhanced Raman Spectroscopy. *J. Am. Chem. Soc.* **2010**, *132*, 10903–10910.
2. Oubre, C.; Nordlander, P. Finite-Difference Time-Domain Studies of the Optical Properties of Nanoshell Dimers. *J. Phys. Chem. B* **2005**, *109*, 10042–10051.
3. Mcmahon, J. M.; Henry, A.-I.; Wustholz, K. L.; Natan, M. J.; Freeman, R. G.; Van Duyne, R. P.; Schatz, G. C. Gold Nanoparticle Dimer Plasmonics: Finite Element Method Calculations of the Electromagnetic Enhancement to Surface-Enhanced Raman Spectroscopy. *Anal. Bioanal. Chem.* **2009**, *394*, 1819–1825.

4. Hao, E.; Schatz, G. C. Electromagnetic Fields around Silver Nanoparticles and Dimers. *J. Chem. Phys.* **2004**, *120*, 357–366.
5. Camden, J. P.; Dieringer, J. A.; Wang, Y.; Masiello, D. J.; Marks, L. D.; Schatz, G. C.; Van Duyne, R. P. Probing the Structure of Single-Molecule Surface-Enhanced Raman Scattering Hot Spots. *J. Am. Chem. Soc.* **2008**, *130*, 12616–12617.
6. Michaels, A. M.; Nirmal, M.; Brus, L. E. Enhanced Raman Spectroscopy of Individual Rhodamine 6G Molecules on Large Ag Nanocrystals. *J. Am. Chem. Soc.* **1999**, *121*, 9932–9939.
7. Michaels, A. M.; Jiang, J.; Brus, L. Ag Nanocrystal Junctions as the Site for Surface-Enhanced Raman Scattering of Single Rhodamine 6G Molecules. *J. Phys. Chem. B* **2000**, *104*, 11965–11971.
8. Stranahan, S. M.; Willets, K. A. Super-Resolution Optical Imaging of Single-Molecule SERS Hot Spots. *Nano Lett.* **2010**, *10*, 3777–3784.
9. Weber, M. L.; Willets, K. A. Correlated Super-Resolution Optical and Structural Studies of Surface-Enhanced Raman Scattering Hot Spots in Silver Colloid Aggregates. *J. Phys. Chem. Lett.* **2011**, *2*, 1766–1770.
10. Cang, H.; Labno, A.; Lu, C.; Yin, X.; Liu, M.; Gladden, C.; Liu, Y.; Zhang, X. Probing the Electromagnetic Field of a 15-Nanometre Hotspot by Single Molecule Imaging. *Nature* **2011**, *469*, 385–388.
11. Henglein, A.; Giersig, M. Formation of Colloidal Silver Nanoparticles: Capping Action of Citrate. *J. Phys. Chem. B* **1999**, *103*, 9533–9539.
12. Kerker, M.; Siiman, O.; Bumm, L. A.; Wang, D. S. Surface Enhanced Raman Scattering (SERS) of Citrate Ion Adsorbed on Colloidal Silver. *Appl. Opt.* **1980**, *19*, 3253–3255.
13. Munro, C. H.; Smith, W. E.; Garner, M.; Clarkson, J.; White, P. C. Characterization of the Surface of a Citrate-Reduced Colloid Optimized for Use as a Substrate for Surface-Enhanced Resonance Raman Scattering. *Langmuir* **1995**, *11*, 3712–3720.
14. Sirimuthu, N. M. S.; Bell, S. E. J. Surface-Enhanced Raman Spectroscopy as a Probe of Competitive Binding by Anions to Citrate-Reduced Silver Colloids. *J. Phys. Chem. A* **2005**, *109*, 7405–7410.
15. Ciou, S.-H.; Cao, Y.-W.; Huang, H.-C.; Su, D.-Y.; Huang, C.-L. SERS Enhancement Factors Studies of Silver Nanoprism and Spherical Nanoparticle Colloids in the Presence of Bromide Ions. *J. Phys. Chem. C* **2009**, *113*, 9520–9525.
16. Draine, B. T.; Flatau, P. J. Discrete-Dipole Approximation for Scattering Calculations. *J. Opt. Soc. Am. A* **1994**, *11*, 1491–1499.
17. Cheezum, M. K.; Walker, W. F.; Guilford, W. H. Quantitative Comparison of Algorithms for Tracking Single Fluorescent Particles. *Biophys. J.* **2001**, *81*, 2378–2388.
18. Yildiz, A.; Forkey, J. N.; McKinney, S. A.; Ha, T.; Goldman, Y. E.; Selvin, P. R. Myosin V Walks Hand-over-Hand: Single Fluorophore Imaging with 1.5-nm Localization. *Science* **2003**, *300*, 2061–2065.
19. Yildiz, A.; Selvin, P. R. Fluorescence Imaging with One Nanometer Accuracy: Application to Molecular Motors. *Acc. Chem. Res.* **2005**, *38*, 574–582.
20. Lee, P. C.; Meisel, D. Adsorption and Surface-Enhanced Raman of Dyes on Silver and Gold Sols. *J. Phys. Chem.* **1982**, *86*, 3391–3395.
21. Le Ru, E. C.; Meyer, M.; Etchegoin, P. G. Proof of Single-Molecule Sensitivity in Surface Enhanced Raman Scattering (SERS) by Means of a Two-Analyte Technique. *J. Phys. Chem. B* **2006**, *110*, 1944–1948.
22. Kneipp, K.; Wang, Y.; Dasari, R. R.; Feld, M. S. Single Molecule Detection Using Surface-Enhanced Resonance Raman Scattering (SERRS): A Study Using Rhodamine 6G on Colloidal Silver. *Appl. Spectrosc.* **1995**, *49*, 780–784.
23. Dieringer, J. A.; Lettan, R. B., II; Scheidt, K. A.; Van Duyne, R. P. A Frequency Domain Existence Proof of Single-Molecule Surface-Enhanced Raman Spectroscopy. *J. Am. Chem. Soc.* **2007**, *129*, 16249–16256.
24. Talley, C. E.; Jackson, J. B.; Oubre, C.; Grady, N. K.; Hollars, C. W.; Lane, S. M.; Huser, T. R.; Nordlander, P.; Halas, N. J. Surface-Enhanced Raman Scattering from Individual Au Nanoparticles and Nanoparticle Dimer Substrates. *Nano Lett.* **2005**, *5*, 1569–1574.
25. Ausman, L. K.; Schatz, G. C. On the Importance of Incorporating Dipole Reradiation in the Modeling of Surface-Enhanced Raman Scattering from Spheres. *J. Chem. Phys.* **2009**, *131*, 084708/1–084707/10.
26. Xu, H.; Kall, M. Polarization-Dependent Surface-Enhanced Raman Spectroscopy of Isolated Silver Nanoaggregates. *Chem. Phys. Chem.* **2003**, *4*, 1001–1005.
27. Yoshida, K.-i.; Itoh, T.; Tamaru, H.; Biju, V.; Ishikawa, M.; Ozaki, Y. Quantitative Evaluations of Electromagnetic Enhancement in Surface-Enhanced Resonance Raman Scattering from Plasmonic Properties and Morphologies of Individual Ag Nanostructures. *Phys. Rev. B* **2010**, *81*, 115406/1-9.
28. Yang, W.-H.; Schatz, G. C.; Van Duyne, R. P. Discrete Dipole Approximation for Calculating Extinction and Raman Intensities for Small Particles with Arbitrary Shapes. *J. Chem. Phys.* **1995**, *103*, 869–875.
29. Kelly, K. L.; Coronado, E.; Zhao, L. L.; Schatz, G. C. The Optical Properties of Metal Nanoparticles: The Influence of Size, Shape, and Dielectric Environment. *J. Phys. Chem. B* **2003**, *107*, 668–677.
30. Le Ru, E. C.; Etchegoin, P. G. Rigorous Justification of the $|E|^4$ Enhancement Factor in Surface Enhanced Raman Spectroscopy. *Chem. Phys. Lett.* **2006**, *243*, 63–66.
31. Stranahan, S. M.; Titues, E. J.; Willets, K. A. SERS Orientational Imaging of Silver Nanoparticle Dimers. *J. Phys. Chem. Lett.* **2011**, *2*, 2711–2715.
32. Li, Z.; Shegai, T.; Haran, G.; Xu, H. Multiple-Particle Nanoantennas for Enormous Enhancement and Polarization Control of Light Emission. *ACS Nano* **2009**, *3*, 637–642.
33. Shegai, T.; Li, Z.; Dadosh, T.; Zhang, Z.; Xu, H.; Haran, G. Managing Light Polarization *via* Plasmon–Molecule Interactions within an Asymmetric Metal Nanoparticle Trimer. *Proc. Natl. Acad. Sci. U.S.A.* **2008**, *105*, 16448–16453.
34. Kall, M.; Xu, H.; Johansson, P. Field Enhancement and Molecular Response in Surface-Enhanced Raman Scattering and Fluorescence Spectroscopy. *J. Raman Spectrosc.* **2005**, *36*, 510–514.
35. Litz, J. P.; Camden, J. P.; Masiello, D. J. Spatial, Spectral, and Coherence Mapping of Single-Molecule SERS Active Hot Spots *via* the Discrete-Dipole Approximation. *J. Phys. Chem. Lett.* **2011**, *2*, 1695–1700.
36. Bosnick, K. A.; Jiang, J.; Brus, L. E. Fluctuations and Local Symmetry in Single-Molecule Rhodamine 6G Raman Scattering on Silver Nanocrystal Aggregates. *J. Phys. Chem. B* **2002**, *106*, 8096–8099.
37. Johansson, P.; Xu, H.; Kall, M. Surface-Enhanced Raman Scattering and Fluorescence near Metal Nanoparticles. *Phys. Rev. B* **2005**, *72*, 035427\1–17.
38. Fort, E.; Gresillon, S. Surface Enhanced Fluorescence. *J. Phys. D: Appl. Phys.* **2007**, *41*, 1–31.
39. Lakowicz, J. R. Radiative Decay Engineering 5: Metal-Enhanced Fluorescence and Plasmon Emission. *Anal. Biochem.* **2005**, *337*, 171–194.
40. McLellan, J. M.; Li, Z.-Y.; Siekkinen, A. R.; Xia, Y. The SERS Activity of a Supported Ag Nanocube Strongly Depends on Its Orientation Relative to Laser Polarization. *Nano Lett.* **2007**, *7*, 1013–1017.
41. Mohamed, M. B.; Volkov, V.; Link, S.; El-Sayed, M. A. The "Lightning" Gold Nanorods: Fluorescence Enhancement of over a Million Compared to the Gold Metal. *Chem. Phys. Lett.* **2000**, *317*, 517–523.
42. Geddes, C. D.; Parfenov, A.; Gryczynski, I.; Lakowicz, J. R. Luminescent Blinking from Silver Nanostructures. *J. Phys. Chem. B* **2003**, *107*, 9989–9993.
43. Andersen, P. C.; Jacobson, M. L.; Rowlen, K. L. Flashy Silver Nanoparticles. *J. Phys. Chem. B* **2004**, *108*, 2148–2153.
44. Boyd, G. T.; Yu, Z. H.; Shen, Y. R. Photoinduced Luminescence from the Noble Metals and Its Enhancement on Roughened Surfaces. *Phys. Rev. B* **1986**, *33*, 7923–7936.
45. Yeshchenko, O. A.; Dmitruk, I. M.; Alexeenko, A. A.; Losytskyy, M. Y.; Kotko, A. V.; Pinchuk, A. O. Size-Dependent

Surface-Plasmon-Enhanced Photoluminescence from Silver Nanoparticles Embedded in Silica. *Phys. Rev. B* **2009**, *79*, 235438\1-8.
46. Zhang, A.; Zhang, J.; Fang, Y. Photoluminescence from Colloidal Silver Nanoparticles. *J. Lumin.* **2008**, *128*, 1635–1640.
47. Itoh, T.; Kikkawa, Y.; Biju, V.; Ishikawa, M.; Ikehata, A.; Ozaki, Y. Steady-State and Time-Resolved Background Luminescence from Surface-Enhanced Resonance Raman Scattering-Active Single Ag Nanoaggregates. *J. Phys. Chem. B* **2006**, *110*, 21536–21544.
48. Harb, M.; Rabilloud, F.; Simon, D.; Rydlo, A.; Lecoultre, S.; Conus, F.; Rodrigues, V.; Felix, C. Optical Absorption of Small Silver Clusters: Ag_n, (n=4−22). *J. Chem. Phys.* **2008**, *129*, 194108\1-9.
49. Borys, N. J.; Lupton, J. M. Surface-Enhanced Light Emission from Single Hot Spots in Tollens Reaction Silver Nanoparticle Films: Linear *versus* Nonlinear Optical Excitation. *J. Phys. Chem. C* **2011**, *115*, 13645–13659.
50. Peyser, L. A.; Vinson, A. E.; Bartko, A. P.; Dickson, R. M. Photoactivated Fluorescence from Individual Silver Nanoclusters. *Science* **2001**, *291*, 103–106.
51. Peyser, L. A.; Lee, T.-H.; Dickson, R. M. Mechanism of Ag_n Nanocluster Photoproduction from Silver Oxide Films. *J. Phys. Chem. B* **2002**, *106*, 7725–7728.
52. Lee, T.-H.; Gonzalez, J. I.; Dickson, R. M. Strongly Enhanced Field-Dependent Single-Molecule Electroluminescence. *Proc. Natl. Acad. Sci. U.S.A.* **2002**, *99*, 10272–10275.
53. Jiang, J.; Bosnick, K.; Maillard, M.; Brus, L. Single Molecule Raman Spectroscopy at the Junctions of Large Ag Nanocrystals. *J. Phys. Chem. B* **2003**, *107*, 9964–9972.
54. Itai, K. Theory of Raman Scattering in Coupled Electron-Phonon Systems. *Phys. Rev. B* **1992**, *45*, 707–717.
55. Zawadowski, A.; Cardona, M. Theory of Raman Scattering on Normal Metals with Impurities. *Phys. Rev. B* **1990**, *42*, 10732–10734.
56. Geddes, C. D.; Parfenov, A.; Gryczynski, I.; Lakowicz, J. R. Luminescent Blinking of Gold Nanoparticles. *Chem. Phys. Lett.* **2003**, *380*, 269–272.
57. Norrod, K. L.; Rowlen, K. L. Removal of Carbonaceous Contamination from SERS-Active Silver by Self-Assembly of Decanethiol. *Anal. Chem.* **1998**, *70*, 4218–4221.
58. Cui, Y.; Wang, W.; Liu, R.; Sun, Z.; Wei, Y.; Zhao, Y.; Gao, X. Serial Silver Clusters Biomineralized by One Peptide. *ACS Nano* **2011**, *5*, 8684–8689.
59. Petty, J. T.; Story, S. P.; Juarez, S.; Votto, S. S.; Herbst, A. G.; Degtyareva, N. N.; Sengupta, B. Optical Sensing by Transforming Chromophoric Silver Clusters in DNA Nanoreactors. *Anal. Chem.* **2012**, *84*, 356–364.
60. Diez, I.; Ras, R. H. A. Fluorescent Silver Nanoclusters. *Nanoscale* **2011**, *3*, 1963–1970.
61. Wang, Z.; Palmer, R. E. Mass Spectrometry and Dynamics of Gold Adatoms Observed on the Surface of Size-Selected Au Nanoclusters. *Nano Lett.* **2012**, *12*, 91–95.
62. Gass, A. N.; Kapusta, O. I.; Klimin, S. A.; Mal'shukov, A. G. The Nature of the Inelastic Background in Surface Enhanced Raman Scattering Spectra of Coldy-Deposited Silver Films. The Role of Active Sites. *Solid State Commun.* **1989**, *71*, 749–753.
63. Portales, H.; Duval, E.; Saviot, L.; Fujii, M.; Sumitomo, M.; Hayashi, S. Raman Scattering by Electron−Hole Excitations in Silver Nanocrystals. *Phys. Rev. B* **2001**, *63*, 233402\1-4.
64. Otto, A. Theory of First Layer and Single Molecule Surface Enhanced Raman Scattering (SERS). *Phys. Status Solidi A* **2001**, *188*, 1455–1470.